

Exact diagonalization using hierarchical wave functions and calculation of topological entanglement entropy

Deepak Gaur,^{1,2} Hrushikesh Sable,^{1,*} and D. Angom³

¹*Physical Research Laboratory, Ahmedabad - 380009, Gujarat, India*

²*Indian Institute of Technology Gandhinagar, Palaj, Gandhinagar - 382355, Gujarat, India*

³*Department of Physics, Manipur University, Canchipur - 795003, Manipur, India*

In this work we describe a new technique for numerical exact diagonalization. The method is particularly suitable for cold bosonic atoms in optical lattices, in which multiple atoms can occupy a lattice site. We describe the use of the method for Bose-Hubbard model of a two-dimensional square lattice system as an example; however, the method is general and can be applied to other lattice models and can be adapted to three-dimensional systems. The proposed numerical technique focuses in detail on how to construct the basis states as a hierarchy of wave functions. Starting from single-site Fock states, we construct the basis set in terms of row states and multirow states. This simplifies the application of constraints and calculation of the Hamiltonian matrix. The approach simplifies the calculation of the reduced density matrices, and this has applications in characterizing the topological entanglement of the state. Each step of the method can be parallelized to accelerate the computation. As a case study, we discuss the computation of the spatial bipartite entanglement entropy in the correlated $\nu = 1/2$ fractional quantum Hall state.

I. INTRODUCTION

Very few problems in quantum many-body systems are analytically solvable. One often resorts to numerical techniques to gain insights on these systems. Numerical mean-field methods are straightforward and easy to use [1]; however, they fail to accommodate the correlations and entanglement of a quantum system. The quantum Monte Carlo (QMC)-based methods like the stochastic series expansion [2, 3] are powerful numerical techniques. These are often used to study the properties of the system in thermodynamic limit. However, for fermionic systems, QMC suffers from the “sign problems” [4]. In addition, a direct access to the full quantum state is not possible with QMC. To obtain the complete information of the system, the numerical exact-diagonalization (ED) is accurate and dependable. As the name suggests, the Hamiltonian matrix is “exactly” diagonalized after choosing an appropriate basis, and generating the Hamiltonian matrix with the basis states. For most of the studies on quantum-mechanical systems at low temperatures, the low-energy states, namely, the ground state and few excited states, are sufficient to describe the important properties. This simplicity allows the usage of the Lanczos algorithm for faster numerical diagonalization [5, 6]. Although ED offers the advantage of access to the exact solution, it is however, computation intensive and grows with complexity of the problem. For instance, for spins on a lattice, the Hilbert space of the system grows exponentially with the lattice size. Thus, ED limits the system size that one can study. In the literature there exists large-scale ED studies for spin-1/2 kagome Heisenberg antiferromagnet with $\approx 40 - 50$ spins [7, 8], bosonic fractional quantum Hall on a 12×4 lattice [9].

In this work, we introduce an ED-based method well suited for ultracold bosons in optical lattices. These quantum sys-

tems serve as excellent quantum simulators to study various condensed-matter systems [10], as they allow remarkable control and tunability of system parameters in experiments [11, 12]. The Bose-Hubbard model (BHM) is a prototypical model which describes the low-energy physics of these systems [13–15]. The mean-field methods like the Gutzwiller mean-field theory [16–18] provide qualitative insights, but do not represent the correlations accurately. One area where ED has provided detailed insights and reliable results is in identifying topological phases like the quantum Hall states. Such states can be experimentally realized with the ultracold atoms by introducing synthetic gauge fields [19–21]. Mean-field methods are not suitable for studying these strongly correlated phases. There are various proposals to realize bosonic analogues of fractional quantum Hall (FQH) states [22–25]. Recently, a $\nu = 1/2$ bosonic FQH state was experimentally observed with ultracold atoms [26]. A rudimentary version of the proposed ED method, as a component of the cluster Gutzwiller mean-field theory implementation, was employed in our previous works to analyze the quantum phases in an optical lattice for a wide variety of systems. These include bosonic quantum Hall phase [9, 27, 28], Bose-glass phase [29], supersolid phase in dipolar bosons [30, 31], dipolar bosonic mixtures [32], dipolar bosons in multilayer optical lattice [33].

The ED method we have developed relies on a hierarchical sequence of basis states. The single-site Fock states constitute the lowest hierarchy of the sequence. Next, the tensor products of these states define a 1D or row state. Finally, the tensor product of the row states, referred to as the multirow states, form the basis set of the ED method. This approach facilitates applying constraints on the system, such as restrictions on the occupancies in the rows and system as a whole [9]. Once the basis states, also referred interchangeably as cluster states, are generated, calculation of the Hamiltonian matrix is the next step in ED. For lattice systems the Hamiltonian matrix is, in general, sparse. We take advantage of this feature and calculate only the nonzero elements by identifying the nonzero

* Present address: Department of Physics, Virginia Tech, Blacksburg, Virginia 24061, USA

elements corresponding to a cluster state. This, however, requires a more sophisticated approach when constraints are included. We then develop and present appropriate schemes to calculate bipartite entanglement entropy, which requires partitioning the system into two distinct subsystems. It is a good measure of correlations in a quantum state [34, 35] and valuable in studying quantum Hall states.

We have organized the remainder of this article as follows. In Sec. II we describe our implementation of the ED technique in terms of row states as the fundamental building blocks. We describe the construction of the set of basis states and that of the Hamiltonian in this section. This is followed by Sec. III, where we discuss the modified construction procedures when additional constraints are imposed for filtering out the basis states. These constraints reduce the size of the Hilbert space. In Sec. IV we establish the validity of our ED method and benchmark it by calculating selected ground-state properties of BHM. In Sec. V we demonstrate the usage of the algorithm for studying the spatial bipartite entanglement in the $\nu = 1/2$ bosonic FQH state. Finally, we conclude in Sec. VI.

II. COMPLETE BASIS SET

Consider a system of ultracold bosonic atoms loaded in a two-dimensional (2D) optical lattice and to simplify the description, consider the geometry to be square. Such a system is well described by the Bose-Hubbard Hamiltonian given by

$$\hat{H}_{\text{BHM}} = \sum_{p,q} \left[-J \left(\hat{b}_{p+1,q}^\dagger \hat{b}_{p,q} + \hat{b}_{p,q+1}^\dagger \hat{b}_{p,q} + \text{H.c.} \right) + \frac{U}{2} \hat{n}_{p,q} (\hat{n}_{p,q} - 1) \right], \quad (1)$$

where p (q) is the lattice site index along the x (y) direction, $\hat{b}_{p,q}$ ($\hat{b}_{p,q}^\dagger$) is the annihilation (creation) operator at lattice site (p, q) , $\hat{n}_{p,q}$ is the number operator, and U is the on-site interaction strength. The eigenstate of a system with a size of $K \times L$ can be written as the linear combination,

$$|\Psi\rangle = \sum_{\substack{n_{1,1} \\ \vdots \\ n_{p,q} \\ \vdots \\ n_{K,L}}} C_{n_{1,1}, \dots, n_{p,q}, \dots, n_{K,L}} |n_{1,1}, \dots, n_{p,q}, \dots, n_{K,L}\rangle, \quad (2)$$

where $n_{p,q}$ is the occupancy at the lattice site (p, q) , and K (L) is the number of lattice sites along the x (y) direction. To obtain the ground state or any other excited states, the coefficients $C_{n_{1,1}, \dots, n_{p,q}, \dots, n_{K,L}}$ corresponding to the basis state $|n_{1,1}, \dots, n_{p,q}, \dots, n_{K,L}\rangle$ must be defined. The basis states are defined in terms of a hierarchy of multiple lattice sites, with the starting point being the single-site Fock states.

A. Construction of the basis states

As mentioned earlier, the occupancy of a lattice site (p, q) is denoted by $n_{p,q}$, and the corresponding Fock state can

be represented as $|n_{p,q}\rangle$. Although $n_{p,q}$ can in principle be any non-negative integer, let us consider only N_B possible choices $n_{p,q} \in \{0, 1, 2, \dots, N_B - 1\}$. A configuration of occupancies of lattice sites along the q th row can then be collectively represented by a ‘‘row state’’, defined as $|n_{1,q}, n_{2,q}, \dots, n_{p,q}, \dots, n_{K,q}\rangle \equiv \prod_{p=1}^K \otimes |n_{p,q}\rangle$, where $1 \leq p \leq K$ is the lattice site index along the row. In general, the label q corresponding to the row can be omitted, as it is common for all the lattice sites along the row. And a row state can be defined as

$$|n_1, n_2, \dots, n_p, \dots, n_K\rangle = \prod_{p=1}^K \otimes |n_p\rangle. \quad (3)$$

The advantage of defining the row states is that any configuration of particles in the entire lattice can be expressed as a direct product of the row states. Thus the row states are the building blocks of the basis states of the entire lattice system.

The occupancies, as mentioned earlier, can be $0 \leq n_p \leq N_B - 1$. Then the total number of possible row-state configurations is $\alpha = (N_B)^K$. Each row-state configuration is uniquely identified by the quantum number m and represented as

$$|\phi_m\rangle \equiv \prod_{p=1}^K |n_p\rangle, \quad (4)$$

with $m \in \{0, 1, 2, \dots, \alpha - 1\}$. The quantum number m and the number of particles (N_m) in the row state are given by

$$m = \sum_{p=1}^K n_p N_B^{p-1}, \text{ and } N_m = \sum_{p=1}^K n_p. \quad (5)$$

Using the row states, we construct multirow states, which are the occupancy configurations in multiple rows. The multirow states of two rows, referred as two-row states, is represented as $|\Phi^2\rangle$. In the present case, the lattice dimension of $|\Phi^2\rangle$ is $(K \times 2)$, and each of the two-row states is a direct product of the row states $|\phi_m\rangle$, defined in Eq. (4) as

$$|\Phi_M^2\rangle = |\phi_{m_2}\rangle \otimes |\phi_{m_1}\rangle. \quad (6)$$

Here, the label M corresponds to a two-dimensional vector $\mathbf{M} = (m_1, m_2)$. It contains information about the row states which constitutes the two-row state. Thus, the total number of possible two-row states is α^2 , and for a combination of m_1 and m_2 , the corresponding state label is $M = \alpha(m_1) + m_2$. Similarly, multirow states of a higher number of rows can be constructed from the direct product of multirow states with fewer number of rows and row states, as

$$\begin{aligned} |\Phi_{M'}^3\rangle &= |\Phi_M^2\rangle \otimes |\phi_m\rangle, \\ |\Phi_{M'}^4\rangle &= |\Phi_M^3\rangle \otimes |\phi_m\rangle. \end{aligned} \quad (7)$$

Considering the hierarchy of the multirow states, different rank multirow states with q rows $|\Phi_M^q\rangle$ is identified by a vector $\mathbf{M} = (m_1, m_2, \dots, m_q)$ in a q -dimensional space. The row-state quantum numbers are the components of the vector,

and each axes represents one of the row states. Various q -row states are assigned a unique integer index M corresponding to the vector label \mathbf{M} , and the number of particles in the state N_M are

$$M = \sum_{j=1}^q m_j (N_B)^{K(L-j)}, \text{ and } N_M = \sum_{p=1}^K \sum_{q'=1}^q n_{p,q'}. \quad (8)$$

Generalizing the definition of multirow states, the basis states of a system with L rows and K columns is constructed as a direct product of two appropriately chosen multirow states. Each of the basis states $|\Phi_M^L\rangle$ is identified by an L -dimensional vector $\mathbf{M} = (m_1, m_2, \dots, m_L)$ and an index M . For example, the basis for a $K \times 7$ lattice system can be constructed as a direct product of multirow states $|\Phi_{M_1}^4\rangle$ and $|\Phi_{M_2}^3\rangle$ as given below:

$$|\Phi_M^7\rangle = |\Phi_{M_1}^4\rangle \otimes |\Phi_{M_2}^3\rangle. \quad (9)$$

The basis states are uniquely identified by a vector \mathbf{M} and are labeled with an integer M according to relation given in Eq. (8). Thus, in general the basis states of $K \times L$ can be defined as the direct product

$$|\Phi_M^L\rangle = |\Phi_{M_1}^{L_1}\rangle \otimes |\Phi_{M_2}^{L_2}\rangle, \quad (10)$$

where $L = L_1 + L_2$. Below is a schematic representation showing the occupancies over the lattice which constitutes a basis state, being identified as a column vector of row states, which is the essence of Eq. (9):

$$\begin{pmatrix} n_{1,L} & n_{2,L} & \cdots & n_{p,L} & \cdots & n_{K,L} \\ \vdots & \vdots & & \vdots & & \vdots \\ n_{1,q} & n_{2,q} & \cdots & n_{p,q} & \cdots & n_{K,q} \\ \vdots & \vdots & & \vdots & & \vdots \\ n_{1,2} & n_{2,2} & \cdots & n_{p,2} & \cdots & n_{K,2} \\ n_{1,1} & n_{2,1} & \cdots & n_{p,1} & \cdots & n_{K,1} \end{pmatrix} \equiv \begin{pmatrix} m_L \\ \vdots \\ m_q \\ \vdots \\ m_2 \\ m_1 \end{pmatrix}.$$

Thus any basis state representing the configuration of particles on a 2D lattice with L rows can be thought of as a point in the L -dimensional hyper-space spanned by the row states $|\phi_{m_j}\rangle$, as shown in Fig. 1. With these definitions, the number of possible basis states of the system is α^L . Using these, any state of the system can be expressed in terms of the basis states as

$$|\psi\rangle = \sum_{M=0}^{\alpha^L-1} C^M |\Phi_M^L\rangle, \quad (11)$$

where C^M is the coefficient corresponding to the basis $|\Phi_M^L\rangle$ in the wave function $|\psi\rangle$. The corresponding vector $\mathbf{M} = (m_1, m_2, \dots, m_L)$ has the information regarding the occupancies along all the rows corresponding to M th basis state.

B. Construction of Hamiltonian matrix

Let us now consider the BHM Hamiltonian given in Eq. (1). Consider the hopping term $-J\hat{b}_{p+1,q}^\dagger \hat{b}_{p,q}$, which describes the

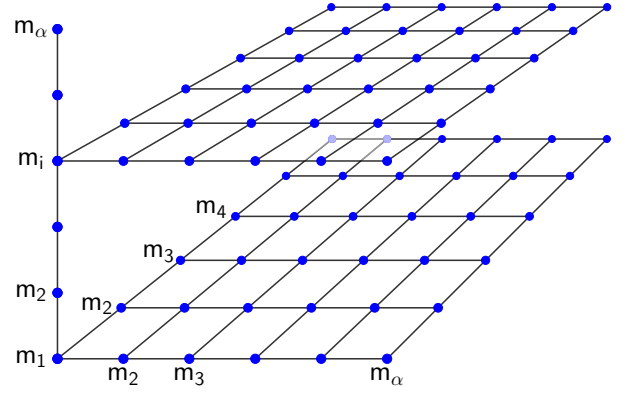


FIG. 1. Schematic illustration of the hyper-space spanned by the row-state quantum numbers along various rows which together constitute the lattice. The basis state are identified by the grid points in the three-dimensional space for a lattice consisting of three rows.

hopping of a particle from the lattice site (p, q) to $(p+1, q)$. The action of this term on a basis state affects only two lattice sites of the q th row. Thus, its operation on the row yields

$$\begin{aligned} & \hat{b}_{p+1,q}^\dagger \hat{b}_{p,q} |n_1, \dots, n_p, n_{p+1}, \dots, n_K\rangle \\ &= \sqrt{n_p (n_{p+1} + 1)} |n_1, \dots, (n_p - 1), (n_{p+1} + 1), \dots, n_K\rangle, \end{aligned}$$

if the hopping is allowed, which corresponds to $n_p - 1 \geq 0$ and $n_{p+1} \leq N_B - 1$. Otherwise, the action of the hopping term results to zero. Thus for a possible hopping, this hopping term only modifies the row state $|\phi_{m_q}\rangle$ to a different row state $|\phi_{m'_q}\rangle$

$$\hat{b}_{p+1,q}^\dagger \hat{b}_{p,q} |\phi_{m_q}\rangle = \sqrt{n_p (n_{p+1} + 1)} |\phi_{m'_q}\rangle, \quad (12)$$

and the quantum numbers of the row states are related as

$$\begin{aligned} m'_q - m_q &= \sum_{j=1}^K (n'_j - n_j) N_B^{j-1}, \\ &= N_B^{p-1} (N_B - 1). \end{aligned} \quad (13)$$

Thus, for a possible x hopping, the operation of the hopping term $-J\hat{b}_{p+1,q}^\dagger \hat{b}_{p,q}$ on the basis state $|\Phi_M^L\rangle$ can be written as

$$-J\hat{b}_{p+1,q}^\dagger \hat{b}_{p,q} |\Phi_M^L\rangle = -J\sqrt{n_{p,q} (n_{p+1,q} + 1)} |\Phi_{M'}^L\rangle, \quad (14)$$

where the corresponding basis states vectors $\mathbf{M} = (m_1, m_2, \dots, m_L)$ and $\mathbf{M}' = (m'_1, m'_2, \dots, m'_L)$ are related as

$$m'_j = \begin{cases} m_j & \text{if } j \neq q, \\ m_q + N_B^{p-1} (N_B - 1) & \text{if } j = q. \end{cases} \quad (15)$$

Here, $n_{p,q}$ is the occupancy at site (p, q) for the basis $|\Phi_M^L\rangle$. Thus we can calculate the nonzero matrix element of the hop-

ping term as

$$\begin{aligned} (-J\hat{b}_{p+1,q}^\dagger \hat{b}_{p,q})_{M'M} &\equiv \langle \Phi_{M'}^L | -J\hat{b}_{p+1,q}^\dagger \hat{b}_{p,q} | \Phi_M^L \rangle, \\ &= -J\sqrt{n_{p,q}(n_{p+1,q}+1)}. \end{aligned} \quad (16)$$

Similarly, consider the hopping term $-J\hat{b}_{p,q+1}^\dagger \hat{b}_{p,q}$, which describes the hopping of particles from lattice site (p, q) to $(p, q+1)$ between two neighboring rows. The hopping term will modify the row states at $q+1$ and q th rows. Thus, for a possible y hopping, the action of the hopping term $-J\hat{b}_{p,q+1}^\dagger \hat{b}_{p,q}$ on the basis state $|\Phi_M^L\rangle$ is given by

$$-J\hat{b}_{p,q+1}^\dagger \hat{b}_{p,q} |\Phi_M^L\rangle = -J\sqrt{n_{p,q}(n_{p,q+1}+1)} |\Phi_{M'}^L\rangle, \quad (17)$$

where

$$m'_j = \begin{cases} m_j & \text{if } j \neq q, j \neq q+1, \\ m_q - N_B^{p-1} & \text{if } j = q, \\ m_{q+1} + N_B^{p-1} & \text{if } j = q+1, \end{cases} \quad (18)$$

and this contributes to the (M', M) Hamiltonian matrix element. In a similar way, the other terms of the Hamiltonian can be evaluated.

III. STATE REDUCTION

The row states $|\phi_m\rangle$ and multirow states $|\Phi_M^q\rangle$ considered so far are without restrictions on the total number of particles $N = \sum_{p=1}^K \sum_{q=1}^L n_{p,q}$, except for the constraint of $n_{p,q}$ not exceeding $N_B - 1$. Thus, the basis states described by Eq. (10) include all possible states with $0 \leq N \leq (N_B - 1)KL$. Such a basis set is not appropriate for calculations with fixed N or in studies using the canonical ensemble for BHM-like Hamiltonians, where the number operator commutes with the Hamiltonian and is thus a conserved quantity. For such cases, let us refine the basis-state construction to impose the constraint of selecting states with a particular value of N . This implies that $n_{p,q}$ can range from 0 to $\min(N, N_B - 1)$. Depending on the problem of interest, additional constraints can be imposed on basis states. For example, at unit filling ($N = K \times L$) average occupancies at each lattice site is 1, and thus basis states with occupancies $n_{p,q} > 2$ may not contribute to the lowest energy sector. So it is appropriate to impose constraints, which reduces the number of the basis states. These considerations, however, require modifications in the basis construction procedure and Hamiltonian matrix calculation.

A. Construction of the row states

The single-site Fock states $|n_{p,q}\rangle$ considered so far have occupancies $0 \leq n_{p,q} \leq (N_B - 1)$. For quantum states with higher average occupancies, it is appropriate to modify the choice of $|n_{p,q}\rangle$ with the constraint

$$\eta \leq n_{p,q} \leq (N_B - 1). \quad (19)$$

This fixes the number of single-site Fock states to $N_B - \eta$ but modifies the lowest possible occupancy of the single-site Fock state to η . The other constraint is to restrict the number of particles in a row state within a range of values,

$$\sigma \leq \sum_{p=1}^K n_{p,q} \leq \sigma + \delta, \quad (20)$$

where $\sigma \geq \eta K$ and $\sigma + \delta \leq (N_B - 1)K$. This sets a limit on the minimum number of particles in a row state as σ and fixes the range to δ . Such a constraint is appropriate to generate basis sets of optimal sizes to study quantum phases with low average occupancies. Further, as the constraint is on the range of N_m , it can also be imposed to limit the basis set size but ensure that it represents the number fluctuation of the quantum phase appropriately. Thus, Eq. (4) can still be used to describe the row states with the constraints in Eqs. (19) and (20). Due to the state-reduction constraints set by Eq. (20), the quantum number m of the selected row states need not be consecutive integers. And thus m is unsuitable as index to identify row states and labeling of the Hamiltonian matrix elements. Consider the set of the selected row-state quantum numbers in ascending order, $\mathcal{S} = \{m_i : m_i < m_{i+1} \text{ and } i, i+1 \in \mathcal{S}'\}$. Here, i is the sequence label, which forms an index set $\mathcal{S}' = \{1, 2, \dots, \beta\}$, and β is the number of the selected row states. As mentioned earlier, m_i and m_{i+1} need not be consecutive integers but are consecutive elements of \mathcal{S} . For better organization and tractability, we redefine the row states with the label i denoted as $|\phi\rangle_i$. This redefinition implies $|\phi\rangle_i \equiv |\phi_{m_i}\rangle$. Appendix A illustrates, as an example, the generation of the row-state configurations for appropriately chosen state reduction constraints. As described earlier, the row states are used to construct the basis for the entire system. To generate the basis set, only the multirow states satisfying the constraints are selected. The selection is simplified by the use of the multirow states, which forms the building block for the construction of the basis states.

B. Multirow states with constraints

The constraints as expressed in Eqs. (19) and (20) are for the single site and row state, respectively. For the entire lattice system, a constraint on N can be imposed as

$$\Sigma \leq \sum_{p=1}^K \sum_{q=1}^L n_{p,q} \leq \Sigma + \Delta, \quad (21)$$

where, $\Sigma \geq \sigma L$ and $\Delta \leq \delta L$. Like in the case of a row state, this sets a limit on the minimum number of particles in a basis state as Σ and fixes the range to Δ . This constraint is suitable when total number of particles in the lattice is not fixed. Thus, to reduce the basis set to an optimal size but appropriate to describe the quantum phase of interest, constraints in Eqs. (19), (20), and (21) are imposed to the single site, row state, and basis state, respectively. It must, however, be mentioned that for studies with the micro-canonical ensemble, the total number of particles is fixed and corresponds to $\Delta = 0$.

As described earlier, the multirow states consisting of q rows are denoted by $|\Phi_M^q\rangle$, with a corresponding q -dimensional vector \mathbf{M} which identifies the row states in the q rows. The two-row states can be constructed as a direct product of the row states $|\phi_{m_1}\rangle$ and $|\phi_{m_2}\rangle$ as

$$|\Phi_M^2\rangle \equiv |\phi_{m_1}\rangle \otimes |\phi_{m_2}\rangle : N_M \leq \Sigma + \Delta. \quad (22)$$

Here, $\mathbf{M} = (m_1, m_2)$ has the row-state quantum numbers of the two contributing row states, satisfying the constraint that the total number of particles in the two-row state can at most be equal to $\Sigma + \Delta$. Furthermore, the number of multirow states can be additionally reduced with the imposition of more complex constraints on N_M . Imposing the constraints in Eqs. (19), (20), and (21) retains only the multirow states satisfying these constraints. This reduces the number of multirow states. Then, like the row-state quantum number m , the multirow state quantum number M of the selected states may not be consecutive integers. For improved representation of the multirow states, we follow the same strategy as in a row state. So, let us consider the set formed by the multirow state quantum numbers in ascending order $\mathcal{S} = \{M_I : M_I < M_{I+1}, \text{ and } I, I+1 \in \mathcal{S}'\}$. Here, I is a sequence label, which forms the index set $\mathcal{S}' = \{1, 2, \dots, \beta^{(2)}\}$, and $\beta^{(2)}$ is the total number of possible two-row states. Each of the two-row states can then be represented as $|\Phi^2\rangle_I \equiv |\Phi_{M_I}^2\rangle$. Then, by knowing M_I , the pair of the constituent row states (m_1, m_2) can be identified. Here, with the constraints it is to be noted that $\beta^{(2)} \leq (\beta)^2$. The total possible multirow states obtained with the constraint on N_M are lower in number compared to the possible combinations of selected row states $|\phi_{m_1}\rangle \otimes |\phi_{m_2}\rangle$. Appendix A illustrates, as an example, the construction of possible two-row state configurations generated from the selected row states. Similarly, the three-row states can be constructed as a direct product of two-row state with label M and a row-state with quantum number m as

$$|\Phi_{M'}^3\rangle \equiv |\Phi_M^2\rangle \otimes |\phi_m\rangle : N_{M'} \leq \Sigma + \Delta. \quad (23)$$

Here, \mathbf{M}' is a vector containing the information of the row-state configurations. And the three-row states, $\beta^{(3)}$ in number, can be similarly identified with an index $I \in \{1, 2, \dots, \beta^{(3)}\}$ and is represented as $|\Phi^3\rangle_I \equiv |\Phi_{M'}^3\rangle$. Following similar steps, states with more number of row states can be constructed.

C. Basis states with constraints

To generate the basis states for the entire lattice system with the constraints, we again use the multirow states as the building blocks. In short, the basis states can be a multirow state or product of two multirow states with an appropriate number of rows. However, only the basis states satisfying the constraint in Eq. (21) are selected. Consider the case of $L = 3$ as an example. The basis states which satisfy the constraint in Eq. (21) are to be selected from the set $\{|\Phi_M^3\rangle\}$, and the members of this set are generated with the constraints in Eqs. (19), (20), and (22). Let

$$|\Phi_{M'}^3\rangle \equiv |\Phi^3\rangle_I \in \{|\Phi_M^3\rangle\} : \Sigma \leq N_{M'} \leq \Sigma + \Delta, \quad (24)$$

be one of the three-row states which satisfies all the constraints. Here $N_{M'}$ represents total number of particles in the three-row state. Then the collection of these states forms the desired basis set $\{|\Phi_{M'}^3\rangle\}$. The labeling of the basis states is done similar to the multirow states as described earlier. Thus each basis state is labeled as $|\Phi^L\rangle_I$, with index $I \in \{1, 2, \dots, \Gamma\}$, where $\Gamma \leq \beta^{(3)}$ is the total number of states in $\{|\Phi_{M'}^3\rangle\}$. Similarly, for the case of a larger lattice $L = 5$, we can use the three- and two-row states to generate basis states as

$$|\Phi^5\rangle_I = |\Phi_M^3\rangle \otimes |\Phi_{M'}^2\rangle : \Sigma \leq N_M + N_{M'} \leq \Sigma + \Delta. \quad (25)$$

Once $\{|\Phi^5\rangle_I\}$ is generated, the model Hamiltonian can then be diagonalized to obtain the ground state as a linear combination,

$$|\Psi\rangle = \sum_{I=1}^{\Gamma} C^I |\Phi^L\rangle_I, \quad (26)$$

where C^I is the coefficient corresponding to the contribution of the basis $|\Phi^L\rangle_I$.

D. Calculation of Hamiltonian matrix elements

Consider the BHM Hamiltonian in Eq. (1), and as an example select one of the hopping terms $-J\hat{b}_{p+1,q}^\dagger \hat{b}_{p,q}$. Then, its operation on the row and basis states can be evaluated using the expressions in Eq. (12)-(15). For the I th basis state, $|\Phi^L\rangle_I \equiv |\Phi_R^L\rangle$, with the row-state components given by vector \mathbf{R} , we get

$$-J\hat{b}_{p+1,q}^\dagger \hat{b}_{p,q} |\Phi_R^L\rangle = -J\sqrt{n_{p,q}(n_{p+1,q} + 1)} |\Phi_{R'}^L\rangle. \quad (27)$$

Here, both states $|\Phi_R^L\rangle$ and $|\Phi_{R'}^L\rangle$ are members of the basis set $\{|\Phi^L\rangle_{I''}\}$ obtained with the constraints. From earlier considerations, the row-state quantum numbers of the two basis states $\mathbf{R} = (r_1, r_2, \dots, r_L)$ and $\mathbf{R}' = (r'_1, r'_2, \dots, r'_L)$ are related by $r'_j = r_j$ for $j \neq q$ and $r'_q = r_q + N_B^{p-1}(N_B - 1)$. This uniquely identifies \mathbf{R}' , but the corresponding index I' of $|\Phi_{R'}^L\rangle \equiv |\Phi^L\rangle_{I'}$ is yet unknown. This is due to the lack of an algebraic relation between I' and \mathbf{R}' . Such a relation as in Eq. (8) is applicable when there is no state reduction. Once the indices are known, we can define the Hamiltonian matrix $H_{II'} = \langle \Phi_{R'}^L | H_{\text{BHM}} | \Phi_R^L \rangle$ and continue the process for all the hopping terms in the BHM Hamiltonian to generate the Hamiltonian matrix.

E. Identifying the basis index I' of \mathbf{R}'

For a system with L rows, as mentioned earlier, the I th cluster or basis state satisfying the constraint equations is $|\Phi^L\rangle_I \equiv |\Phi_M^L\rangle$. The corresponding vector label of the state $\mathbf{M} = (m_1, m_2, \dots, m_L)$ has the row-state quantum numbers

I	$(i_1, i_2, \dots, i_{L-1}, i_L)$
1	(1, 1, \dots 1, 1)
2	(1, 1, \dots 1, 2)
\vdots	\vdots
I_1	(1, 1, \dots 1, β)
$I_1 + 1$	(1, 1, \dots 2, 1)
\vdots	\vdots
I_2	(1, 1, \dots 2, β)
\vdots	\vdots
I_3	(1, 1, \dots β , β)
\vdots	\vdots
I_4	(1, β , \dots β , β)
$I_4 + 1$	(2, 1, \dots 1, 1)
\vdots	\vdots
I_5	(2, β , \dots β , β)
\vdots	\vdots
Γ	$(\beta, \beta, \dots, \beta, \beta)$

TABLE I. Table showing the row-state indices i_q of the row-state configurations in all the rows that together constitute the I th basis state.

of the constituent rows as components. This forms a forward map between I and row-state configurations defined in **M**:

$$\begin{aligned} |\Phi^L\rangle_I &\rightarrow |\phi_{m_1}\rangle \otimes |\phi_{m_2}\rangle \cdots \otimes |\phi_{m_L}\rangle, \\ &\equiv |\phi\rangle_{i_1} \otimes |\phi\rangle_{i_2} \cdots \otimes |\phi\rangle_{i_L}. \end{aligned} \quad (28)$$

However, we also require the inverse map. That is, for a given **M** it should be possible to identify the corresponding I . As discussed earlier, this mapping information is required in the calculation of the Hamiltonian matrix. Such a mapping can be established using the structure adopted in the construction of the cluster states and using bisection. Recall that the number of row-state configurations satisfying the constraint is β , and each row state is identified with a quantum number m and a corresponding label i as $|\phi_m\rangle \equiv |\phi\rangle_i$. The cluster states $|\Phi^L\rangle_I$ are identified and sorted in terms of row-state quantum numbers $(m_1, m_2, \dots, m_{L-1}, m_L)$ and corresponding indices $(i_1, i_2, \dots, i_{L-1}, i_L)$. In this notation, the row-state index i_{q+1} varies faster than the i_q with I . As an example, the sequence of the row-state indices for the cluster states are shown in shown in Table I. From Table I it is evident that i_1 varies monotonically with I in the interval $I \in [1, \Gamma]$. However, i_2 varies monotonically with I for the same i_1 . Similarly i_q varies monotonically with I in the limited interval where $(i_1, i_2, \dots, i_{q-1})$ remain unchanged with I . Given the sequence, for a cluster state with the row-state configurations with indices $(i'_1, i'_2, \dots, i'_L)$, the corresponding cluster state index I' can be identified using a set of bisection searches.

Let us suppose that we have a basis state with row-state configuration $\mathbf{R}' = (r'_1, r'_2, \dots, r'_L)$ and labels $(i'_1, i'_2, \dots, i'_L)$, and we have to identify the corresponding state index I' from

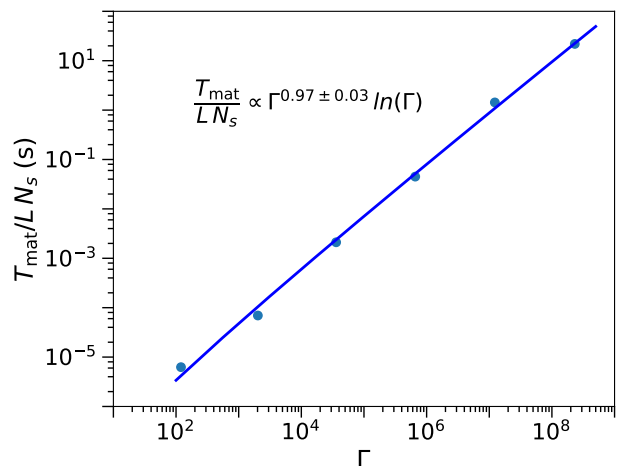


FIG. 2. Scaling of the matrix computation time (T_{mat}) with the size of the basis set Γ . The filled circles corresponds to the T_{mat} of our code, and the solid line is the fitted curve.

the basis set. To accomplish this, we perform a search using the method of bisection in the interval $I \in [1, \Gamma]$. Considering that the leftmost index i_1 as the slowest varying index, we start the bisection to identify the range of basis set index $I \in [I_{\min}^1, I_{\max}^1]$, which has i'_1 as the leftmost row-state index within the basis set. Next, a bisection search is done within this range to locate the range $[I_{\min}^2, I_{\max}^2]$ which has the row-state index i'_2 . At this stage all the basis states within the range $[I_{\min}^2, I_{\max}^2]$ have the same i'_1 and i'_2 as the desired state \mathbf{R}' . We continue the bisection further for each of the row-state indices, and the required basis-state index I' is obtained in the last bisection with the identification of the i'_L . Thus the inverse map needed for locating the basis index from row-state configurations can be achieved through a sequence of L bisection searches. It should be noted that each bisection search requires a maximum of $\log_2(\Gamma)$ comparisons of the row-state index. This is a huge simplification compared to the Γ number of searches required in locating the desired ket with nonzero matrix element, in the brute-force way of spanning over all possible basis states.

Using this method we can, then, generate the Hamiltonian matrix similar to the approach described in Sec. II B. For a state $|\Phi^L\rangle_I$, we identify the I' $\langle \Phi^L |$ which has nonzero matrix element for each of the terms in the Hamiltonian and calculate the matrix element. This generates the Hamiltonian matrix elements along the column corresponding to $|\Phi^L\rangle_I$. Continuing the process for other states, the Hamiltonian matrix can be calculated column wise. It is expected that the computational time T_{mat} involved in the matrix construction scales with the total number of hopping terms in the Hamiltonian, which is proportional to the number of lattice sites N_s . And as mentioned earlier, for each ket state the bra state with a nonzero matrix element is identified in $\sim L \times \ln(\Gamma)$ bisection steps. Thus, it is expected that T_{mat}/N_s should scale as $\sim \Gamma L \ln(\Gamma)$. This dependence is demonstrated in Fig. 2, for the BHM Hamiltonian with hardcore bosons on a 2D lat-

tice of dimension $8 \times L$, with $L \in \{2, 3, 4, 5, 6, 7\}$ and at fixed number density $N/N_s = 1/8$, where different lattice sizes determines the Γ . From the figure it can be noted that $T_{\text{mat}}/N_s \propto \Gamma^{0.97 \pm 0.03} L \ln(\Gamma)$, which is consistent with the scaling relation obtained earlier.

Using the method described, we can calculate the Hamiltonian matrix and diagonalize it to obtain the eigenspectrum and states of the system. To demonstrate the reliability of our ED method, we discuss selected results of BHM computed using the method in the next section.

IV. ED RESULTS FOR GROUND STATE OF BHM

In this section we discuss selected ground-state properties of BHM, computed using our ED method. First, we demonstrate the accuracy of results, and later we discuss the advantage of our method. We highlight the computational advantages of the state reduction.

A. Ground state of BHM at unit filling

In the calculations with softcore bosons, it is essential to introduce a cutoff to the single-site Fock space N_B . This restricts the maximum occupancy of a site. Here, we show that an appropriate N_B can be chosen without affecting the accuracy of the ground state. We demonstrate this by varying N_B and computing the ground-state energy for a 3×3 system with unit average occupancy. As shown in Fig.3(a), the ground state-energy per lattice site E_0 remains unchanged with $N_B \gtrsim 4$. Another property of interest is the inverse participation ratio (IPR) $P_2 = \sum_I |C^I|^4$, which measures the spread of ground state $|\Psi\rangle = \sum_I C^I |\Phi\rangle_I$ among the basis states. As seen from the inset of Fig. 3(a), P_2 remains the same for $N_B \gtrsim 4$, which suggests it as good choice for the cutoff. Further, for a 4×4 system with $J/U = 0.1$ and unit occupancy, the ground-state energy per lattice site is $E_0/U = -0.1176, -0.1318, \text{ and } -0.1321$ for $N_B = 3, 4, \text{ and } 5$, respectively. Here, the change in the energy between $N_B = 4$ and 5 is negligible; thus $N_B \gtrsim 4$ is an appropriate cutoff for $J/U \lesssim 0.1$.

To benchmark our results, we choose $N_B = 4$ for computing the ground-state energy of a 3×3 lattice with unit filling as a function of J/U . The results are shown in Fig.3(b) which are in excellent agreement with the ED results of the same system size reported in Ref. [36]. Furthermore, by increasing the system size to 4×4 , we note that the computed energy approaches the QMC results. We also compute the particle-number correlation function in the ground state of the BHM,

$$F_n(r) = \langle \hat{n}_{\mathbf{r}} \hat{n}_{\mathbf{0}} \rangle - \langle \hat{n}_{\mathbf{r}} \rangle \langle \hat{n}_{\mathbf{0}} \rangle, \quad (29)$$

which measures the density-density correlations between two lattice sites, one of which is fixed at the origin and the other site is located at the coordinate \mathbf{r} . Figure 3(c) shows the variation of $F_n(r)$ for $r = |\mathbf{r} - \mathbf{0}| = 1$ and $\sqrt{2}$ as a function

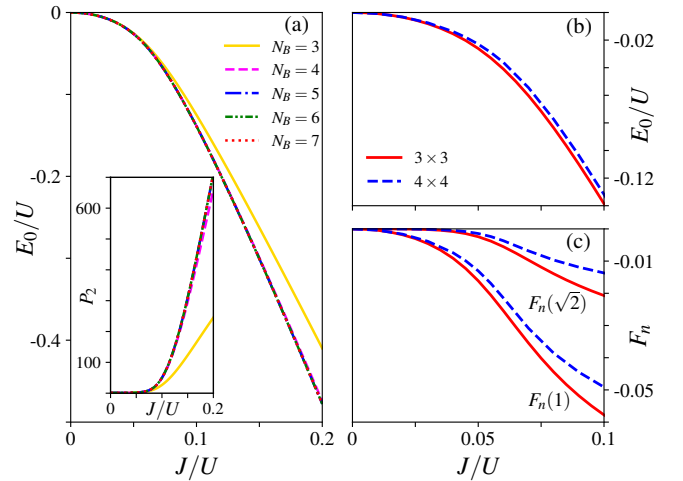


FIG. 3. Ground-state properties of BHM with unit-filling. Panel (a) shows the effect of varying the cutoff in the single-site Fock-space basis size N_B on the energy, and the inset plot corresponds to IPR for a 3×3 system. These quantities are robust for $N_B \gtrsim 4$, as seen from the curves sitting on top of each other for $N_B = 4$ and higher. Panels (b) and (c) show the energy per site E_0/U and the particle-number correlation functions $F_n(r)$, respectively, computed for 3×3 (solid lines) and 4×4 lattices (dashed lines).

of J/U . Here, $r = 1$ and $\sqrt{2}$ correspond to the density correlations between sites which are nearest-neighbors and next-nearest neighbors, respectively. The results of the 3×3 lattice agree with the ED results of the same system size reported in Ref. [36]. And the results of the 4×4 system are close to the QMC data. For further comparisons with QMC results, we compute the ground-state phase diagram of BHM.

B. Phase diagram of BHM

To check the reliability of the method, we next calculate the phase diagram of BHM using the cluster Gutzwiller mean-field (CGMF) method. In the CGMF method, the lattice is tiled with clusters, which are coupled through the mean-field, and the wave function of each cluster is calculated using the exact diagonalization. Thus the diagonalization of a Hamiltonian matrix corresponding to a cluster forms the core of the CGMF method. Consequently, calculation of the phase diagram and comparing with standard results from QMC serves as an important means to check the results obtained using our ED method. More details on the CGMF method are given in Refs.[9, 37]. After rescaling the BHM Hamiltonian with the on-site interaction strength U , we generate the ground-state phase diagram in the μ/U vs J/U plane as shown in Fig. 4. Here, μ is the chemical potential that fixes the total number of particles in the system. As the size of the cluster is increased, the tip of a Mott lobe, which defines the phase boundary between the Mott insulator (MI) and superfluid (SF) phases, shifts to higher J/U . With single-site mean-field method (labeled as 1×1), the tip of the Mott lobe lies at $J_c/U = 0.0429$.

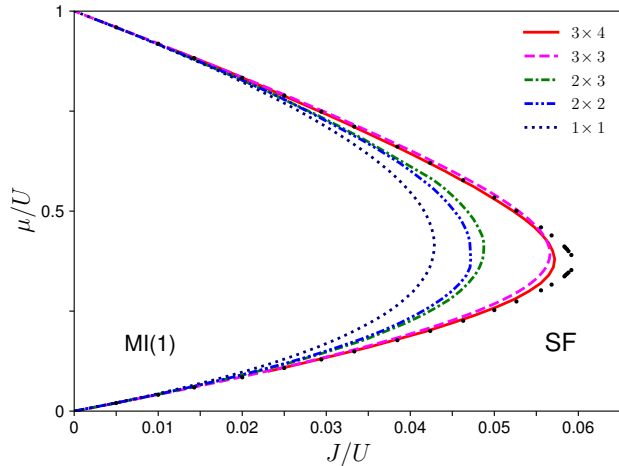


FIG. 4. Phase diagram of BHM computed using CGMF with varying cluster sizes by employing periodic boundary conditions along x and y directions via mean field. The plot corresponding to 1×1 represents data obtained from the single-site mean-field method. For 3×3 and 3×4 clusters, the periodic boundary condition along the x direction is considered as exact hopping. With larger clusters, the Mott lobe approaches the QMC results from Ref. [39], shown with black filled circles [40].

And, with CGMF using a 3×4 cluster, the tip shifts to 0.0572. A cluster-size scaling analysis reported in Ref. [38] gives the location of the tip as $J_c/U = 0.0595$, which is very close to the QMC result of 0.0597 reported in Ref. [39]. Thus, the consistency of the CGMF result with the QMC result directly establishes the accuracy of our method.

C. Computational advantage with our ED method

To benchmark the results of our ED method based on hierarchical wave functions, we compare it with a standard ED library named “quantum basis” available at Github [41]. Using the two codes we check the elapsed time in ED (T_{ED}) as a function of the lattice size and corresponding basis set dimension Γ . For this we chose a system of hardcore bosons at fixed density of $1/4$, for different system sizes 2×4 , 3×4 , \dots , and 9×4 . Additional details of the study are given in Appendix B. The plot comparing the performance of the two codes is shown in Fig. 5. It shows that our code performs better. The basis construction procedure using hierarchical wave functions offers advantages and is better, particularly for larger lattice dimensions. This can be seen from the inset (a) of Fig. 5. For the Hamiltonian matrix construction, both the codes take almost the same duration, which can be seen from the inset (b) of Fig. 5. Similarly, matrix diagonalization takes similar time. This is expected, as both the codes use ARPACK for matrix diagonalization.

To demonstrate the computational advantages with the state reduction, we compute T_{ED} of 4×4 system at unit filling with $N_B = 5$ and $J = 0.1U$. In addition, the accuracy of

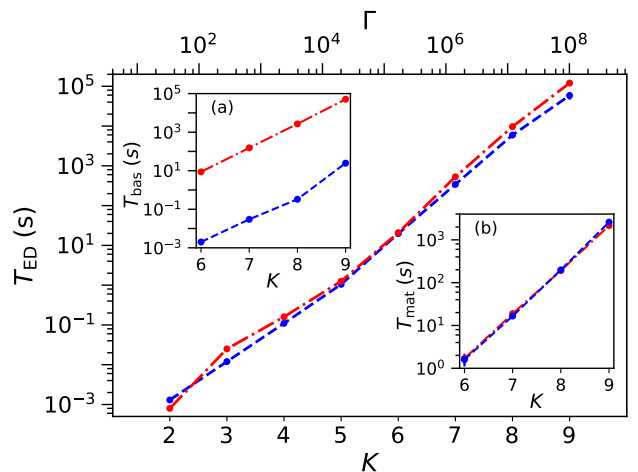


FIG. 5. Comparison of the results from our ED code (dotted curves) with an open-source ED package [41] (dash-dotted curves). The elapsed time in computing the ground state is plotted for a system of hardcore bosons at density $1/4$ on a $K \times 4$ lattice with Γ as total basis states. Inset (a) shows the time taken in the basis construction (T_{bas}), and inset (b) shows the time taken in construction of the Hamiltonian matrix (T_{mat}). In inset (b), the two curves sit on top of each other.

the results with state reduction can be checked by changing the constraints and noting the variations in results. For this, we choose a set of state reductions, introduced in Eq. (20), to constrain the number of bosons of each row by 4 with fluctuations ± 1 , ± 2 , ± 3 , and ± 4 . The trend in T_{ED} with different fluctuations is shown in Fig. 6 (a). The corresponding energies of the ground state (E_0) and first excited state (E_1) are shown in Fig. 6 (b). The figure shows that significant reduction of T_{ED} is achievable without compromising the accuracy of the results.

In the next section we discuss how our ED method can be employed to trace over the spatial degrees of freedom of a wave function when the system is bipartitioned. This can be used in characterizing the entanglement of a state.

V. ENTANGLEMENT IN THE QUANTUM PHASE

The topological characteristics of a system can be inferred by studying the entanglement in the system. It can be used to distinguish a topologically ordered phase like quantum Hall from a normal phase like superfluid. Among various indicators of entanglement in a system, the bipartite entanglement entropy is considered robust. In real-space, it is calculated by partitioning the lattice system into two subsystems, say A and B. The many-body ground-state wave function of the system can then be written in a Schmidt decomposed form as [42]

$$|\Psi\rangle = \sum_j \sqrt{\lambda_j} |\Psi_A\rangle \otimes |\Psi_B\rangle. \quad (30)$$

Here, λ_j are the Schmidt coefficients, and these are the eigenvalues of the reduced density matrix of the subsystem. The re-

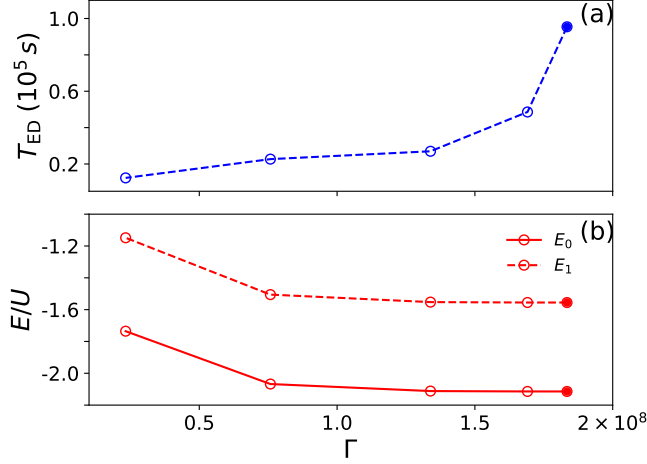


FIG. 6. Comparison of the ED results against the basis set dimensions based on a set of state reductions. For the ground state of a 4×4 system with unit filling, the system parameters are chosen as $N_B = 5$ and $J = 0.1U$. The state reduction constrains the basis states by allowing the total number of bosons in a row to be four with a variation of $\pm 1, \pm 2, \pm 3$, and ± 4 . Open (filled) circles represents the results with (without) state reduction, and solid/dashed lines are visual guide to the eye. Panels (a) and (b) show the elapsed time in ED, and the energies of the ground state (E_0) and first excited state (E_1), respectively.

duced density matrix associated with subsystem A can be obtained from the density matrix after tracing over the degrees of freedom associated with the subsystem B, $\rho_A = \text{Tr}_B |\Psi\rangle\langle\Psi|$. The eigenvalues λ_i of the reduced density matrix give the entanglement spectra, and the bipartite entanglement entropy of the system is the von Neumann entropy associated with the reduced density matrix,

$$S_E = -\text{Tr}[\rho_A \ln \rho_A] = -\sum_j \lambda_j \ln \lambda_j. \quad (31)$$

The entanglement entropy S_E scales with the length (L) of the interface between the two subsystems as [34, 35]

$$S_E = \beta L - \gamma + \mathcal{O}(L^{-\nu}), \quad \nu > 0, \quad (32)$$

where $-\gamma$ is the topological entanglement entropy. It measures the quantum dimension of the quasiparticle excitations in the FQH states. The topologically ordered $\nu = 1/m$ FQH state has $\gamma = 1/2 \ln(m)$. The area-law scaling of the entanglement is typical of ground states for gapped systems [43]. A different way of characterizing the entanglement is to use the geometric entanglement, which does not involve the bipartitioning of the lattice [44].

A. Constructing bipartite reduced density matrix

The approach adopted in the construction of the basis set can be employed in an optimal way to calculate the bipartite reduced density matrix. For this consider partitioning a lattice

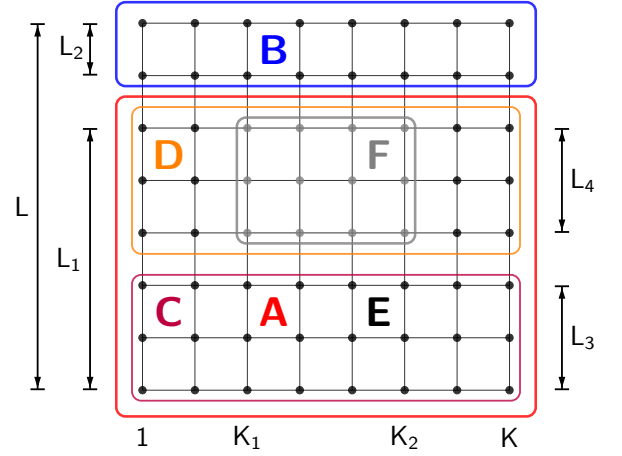


FIG. 7. Visual illustration for the bipartition of the lattice for obtaining the reduced density matrix of subsystem F. First, the lattice is partitioned along the y axis into subsystems A and B. Then subsystem A is further subdivided into subsystems C and D. Finally, subsystem D is partitioned along the x axis to give subsystem F, which comprises the gray-colored lattice sites. The boundaries of the subsystems are identifiable from the corresponding color or shading of the subsystem label. The subsystem E corresponding to the surrounding of subsystem F constitutes the black-colored lattice sites.

system with L rows into two subsystems A and B such that the subsystem A consists of bottom L_1 rows and B consists of top $L_2 = L - L_1$ rows. This is shown schematically in Fig. 7. As each basis state of the lattice consists of L row states, and following Eq. (25), we can write

$$|\Phi_M^L\rangle \equiv |\Phi_{M_1}^{L_1}\rangle \otimes |\Phi_{M_2}^{L_2}\rangle : \Sigma \leq N_{M_1} + N_{M_2} \leq \Sigma + \Delta. \quad (33)$$

Each basis state $|\Phi_M^L\rangle$, labeled with index I , is thus the direct product of multirow states $|\Phi_{M_1}^{L_1}\rangle$ and $|\Phi_{M_2}^{L_2}\rangle$ with labels I_1 and I_2 , respectively. The reduced density matrix ρ_A would then be a $\beta^{(L_1)}$ -dimensional matrix and is obtained after tracing over the degrees of freedom associated with I_2 :

$$\begin{aligned} \rho_A(k, l) &= \sum_{I=1}^{\Gamma} \sum_{I'=1}^{\Gamma} C^{*I} C^{I'} \delta_{I_2, I'_2} \delta_{I_1, k} \delta_{I'_1, l} \\ &= \sum_{I=1}^{\Gamma} \sum_{I'=1}^{\Gamma} \rho(I, I') \delta_{I_2, I'_2} \delta_{I_1, k} \delta_{I'_1, l}. \end{aligned} \quad (34)$$

Here $\rho = |\Psi\rangle\langle\Psi|$ is the density matrix of the system. Similarly, the subsystem A can be further partitioned into two subsystems C and D consisting of bottom L_3 rows and top $L_4 = L_1 - L_3$ rows, respectively. Thus the subsystem state $|\Phi_M^L\rangle$, labeled with index I for $1 \leq I \leq \beta^{(L_1)}$, is the direct product of the state of subsystems C $|\Phi_{M_3}^{L_3}\rangle$ and D $|\Phi_{M_4}^{L_4}\rangle$ with corresponding indices $1 \leq I_3 \leq \beta^{(L_3)}$ and $1 \leq I_4 \leq \beta^{(L_4)}$, respectively. Thus the $\beta^{(L_4)}$ -dimensional

reduced density matrix ρ_D can be obtained as

$$\rho_D(k, l) = \sum_{I=1}^{\beta(L_1)} \sum_{I'=1}^{\beta(L_1)} \rho_A(I, I') \delta_{I_3, I'_3} \delta_{I_4, k} \delta_{I'_4, l}. \quad (35)$$

The bipartitioning of the system discussed so far is by separating along the rows. An example of the partition geometry is as indicated by the sublattices A and B in Fig. 7. However, following ref. [34], the calculation of entanglement entropy requires bipartitioning the system into an isolated and surrounding domains. This is as indicated by the subsystem F and the remaining part E in Fig. 7. In the figure, the gray-colored lattice sites constitute the subsystem F, and the rest of the lattice sites in black constitute the subsystem E. The boundary enclosing the gray-colored lattice sites marks the bipartite separation between subsystems F and E. In this case, the partitioning involves both along rows and columns. To describe the partitioning with a specific example, consider the subdivision of the whole system in Fig. 7 into two, the isolated region F and the remaining part E. To calculate the reduced density matrix of the subsystem F, first the subsystems B and C can be traced out using the method discussed earlier. Then, the required reduced density matrix is obtained by partitioning subsystem D into subsystem F and the remaining lattice sites which forms a part of the subsystem E as shown in Fig. 7. The surrounding of subsystem F corresponds to black-colored lattice sites which constitutes the subsystem E. The partitioning involves tracing out columns on the left and right of subsystem F. Thus, the lattice sites (p, q) for which $L_3 + 1 \leq q \leq L_1$ and $p \in \{K_1, K_1 + 1, \dots, p, \dots, K_2\}$ lie in subsystem F and the rest of the sites are a part of subsystem E over which we wish to trace out. This necessitates the introduction of a unique label corresponding to the different configuration of particles in subsystem F. If the total number of sites in the subsystem F is not large, we can use the following scheme for assigning each configuration with a unique label \tilde{m} given by

$$\tilde{m} = \sum_{q=L_3+1}^{L_1} \sum_{p=K_1}^{K_2} n_{p,q} (N_B)^{(p-K_1)+(L_1-q)(K_2-K_1+1)}. \quad (36)$$

For each multirow state I of subsystem D, the configuration of particles in the subsystem F corresponds to label \tilde{m} given by Eq. (36). For large N_B , the label \tilde{m} can take very large values. This can be circumvented by using the minimal single-site occupancy η as a shift in the occupancies $n_{p,q} \rightarrow n_{p,q} - \eta$ and $N_B \rightarrow N_B - \eta$. Thus, the reduced density matrix of subsystem F can be expressed as

$$\rho_F(k, l) = \sum_{I=1}^{\beta(L_4)} \sum_{I'=1}^{\beta(L_4)} \rho_D(I, I') \delta_{\tilde{m}, k} \delta_{\tilde{m}', l} \prod_{p,q} \delta_{n_{p,q}, n'_{p,q}}, \quad (37)$$

where $n_{p,q}$ and $n'_{p,q}$ are occupancies at the lattice site (p, q) corresponding to the multirow states with indices I and I' , respectively. And the prime on the product over lattice sites (p, q) signifies that product is restricted over only those lattice sites for which $p \in \{1, 2, \dots, K_1 - 1, K_2 + 1, \dots, K\}$ and $q \in \{L_3 + 1, L_3 + 2, \dots, L_1\}$. Alternatively, if the total number

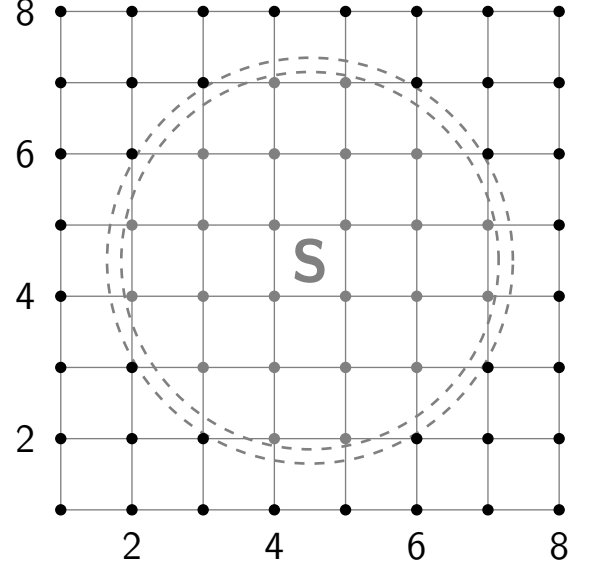


FIG. 8. Visual illustration for spatial bipartitioning of the lattice such that the lattice sites within the circle (gray-colored sites) are chosen as a part of the subsystem S .

of lattice sites in subsystem F is large, then instead of assigning a label to each configuration using Eq. (36), we can construct the multirow states using row states of $K_2 - K_1$ lattice site. And each configuration of particles in subsystem F can then be uniquely identified with the multirow index described earlier. It should be emphasized that the strategy described for obtaining ρ_F is computationally advantageous, since tracing out entire rows can be easily done by utilizing the hierarchical wave functions.

B. Fractional quantum Hall on a lattice

The topological entanglement entropy γ is an appropriate property to distinguish quantum Hall states from the other competing states which are not topological in nature. As an application of the scheme we have developed, we consider the FQH state on a square lattice. The FQH states are supported in the optical lattice with the introduction of synthetic magnetic fields. With this, the hopping term of BHM acquires a lattice-site-dependent Peierls phase. The Hamiltonian of the system in the Landau gauge is given by [45]

$$\hat{H} = \sum_{p,q} \left[\left(-J e^{i2\pi\varphi} \hat{b}_{p+1,q}^\dagger \hat{b}_{p,q} - J \hat{b}_{p,q+1}^\dagger \hat{b}_{p,q} + \text{H.c.} \right) + \frac{U}{2} \hat{n}_{p,q} (\hat{n}_{p,q} - 1) - \mu \hat{n}_{p,q} \right], \quad (38)$$

where φ corresponds to the strength of the magnetic field. We obtain the $\nu = 1/2$ FQH state for a system of four hardcore

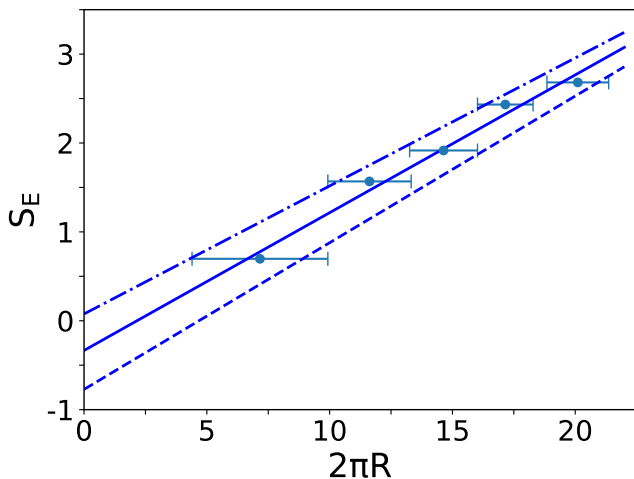


FIG. 9. Entanglement entropy (S_E) of the subsystem S as a function of the length $2\pi R$ of the circular boundary separating S from the rest of the lattice. The plot shows S_E for different subsystem boundary S , and the x error bars represent the ambiguity in the definition of boundary length. The solid, dashed, and dash-dotted lines are the curve obtained by fitting the average, minimum, and maximum values for the boundary length, respectively.

bosons on a 8×8 lattice with periodic boundary conditions and synthetic magnetic field $\varphi = 1/8$. We find the ground state is doubly degenerate, which is an essential property of the $\nu = 1/2$ FQH state on a torus geometry [46]. Using the prescription of Hatsugai [47], we have verified the topological nature of the state and find the many-body Chern number is 1. To calculate γ , we bipartition the lattice system as schematically shown in Fig. 8. Then, we calculate γ between the subsystem S and the rest of the lattice. However, as the lattice is discrete in nature, bipartitioning it with circular geometry introduces an ambiguity in the definition of the boundary as shown in Fig. 8. So, for a given configuration of lattice sites in the subsystem S , we can consider the boundary of the circle enclosing S to lie within the minimum and maximum radii (R_{\min}, R_{\max}). The scaling of S_E with the boundary length L , as shown in Fig. 9, are bounded by two lines, the lower and upper lines corresponding to least-squares fit of data for circles with radii R_{\min} and R_{\max} , respectively. In the figure, the least-squares fit with the average of the two radii is represented by the middle line. We observe that γ , which is the y -intercept, depends on the chosen definition of the boundary length and varies from 0.08 to -0.77 . Considering the average value of the radius $(R_{\min} + R_{\max})/2$, and a least-squares fit, shown as the middle line in Fig. 9 gives $\gamma = 0.33 \pm 0.17$. This value is consistent with the theoretical estimate of $\gamma = \ln \sqrt{2} \approx 0.347$ for a $\nu = 1/2$ Abelian FQH state. The numerical estimates can be improved by incorporating entropy calculations with larger values of L which needs larger lattice dimensions; however, the ambiguity in the definition of L would still be present.

Using the prescription of Kitaev and Preskill for the calculation of γ in terms of the multiple areas, it can be calculated

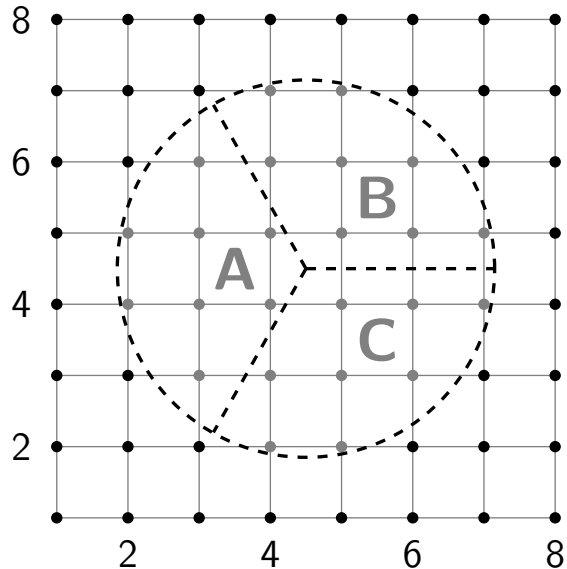


FIG. 10. Visual illustration for spatial bipartitioning of the subsystem in three slices, forming the plural areas. The gray-colored lattice sites, within the dashed circle, are categorized into subsystems A, B, and C.

without the ambiguity of boundary length. In their method γ is given by an appropriate combination of the entanglement entropies of the multiple areas of the subsystem S (shown in Fig. 10) according to the relation $S_{ABC} - S_{AB} - S_{BC} - S_{AC} + S_A + S_B + S_C = -\gamma$ [34]. With this formulation we have calculated γ for various sizes of subsystem S , and the results are shown in Fig. 11. We observe that the numerical estimates of γ are different from the theoretical estimate of -0.35 . However, the trend of γ indicates approaching the theoretical estimate with the larger dimensions of the subsystem S . This can be due to the requirement of a smooth large-sized boundary compared to the correlation length $\xi \ll R$. The estimates of γ can be improved with a larger-sized subsystem on a larger lattice, but the computational resources required is beyond the scope of available computational resources.

VI. DISCUSSIONS

We report the development of a new method on exact diagonalization. It relies on a hierarchy of states to define the basis states of a lattice system. The starting point is the Fock states of the single-lattice sites. Using these, row states are defined as a direct product and then, the product of the row states forms the multirow states. The approach is flexible and it is particularly well suited for studying bosonic optical lattice systems. For such a system, there is no limit on the lattice site occupancy, and the number of basis states grows very fast with the system size and number of particles. In this mul-

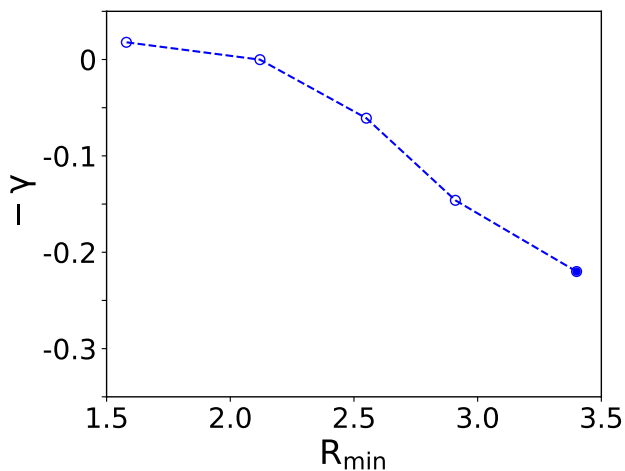


FIG. 11. Topological entanglement entropy ($-\gamma$) obtained for various choices of the circular subsystem S with radii R_{\min} . Open circles correspond to the subsystem S , with the center located at the center of the 8×8 lattice system, and the dashed line is visual guide to the eye. The filled circle corresponds to subsystem S , with the center shifted from the system center.

timestep and hierarchical approach, we can impose various constraints to restrict on the basis set, and this offers an advantage in optimizing the size of the Hamiltonian matrix. The generation of the Hamiltonian matrix is also optimized by identifying the pairs of states which have nonzero matrix elements. For the case of the calculations with constraints, we use the bisection method to accelerate the identification and calculation of the nonzero Hamiltonian matrix elements. All of the constituent steps are parallelizable. In our implementation we have parallelized both the basis set generation and calculation of the Hamiltonian matrix elements. Further more, we parallelize the diagonalization of the Hamiltonian matrix using PARPACK [48]. We benchmark our ED method with calculations of some ground-state properties of BHM. Using the method, we show how to partition a lattice system, compute the reduced density matrix and calculate the topological entanglement entropy. This is applied to the $\nu = 1/2$ FQH state.

VII. ACKNOWLEDGEMENTS

The results presented in this paper were computed on Vikram-100, the 100TFLOP HPC cluster and Param Vikram-1000 HPC cluster at Physical Research Laboratory, Ahmedabad, India. We thank Dr. Rukmani Bai and Dr. Soumik Bandyopadhyay for useful discussions. D.A. would like to acknowledge support from the Science and Engineering Research Board, Department of Science and Technology, Government of India, through Project No. CRG/2022/007099 and support from the UGC through the SAP (DRS-II), Department of Physics, Manipal University.

Appendix A: Example illustration of row states, multirow states and basis-states construction

As an example, consider the states corresponding to an extra particle over the commensurate unit filling state. For this case, we consider a system of 10 bosons on a 3×3 lattice. In order to generate the basis states for this system, we first construct the row states corresponding to the rows comprising of 3 lattice sites. Let us constraint the single-site occupancies such that it can be either 1 or 2. In addition, we filter the possible row-state configurations by imposing the constraint on the total number of particles within a row as either 3 or 4. The possible row-state configurations with these constraints, $\eta = 1$, $N_B = 3$, and $\sigma = 3$ and $\sigma + \delta = 4$ are listed in Table II, where, the row-state configurations $|\phi_m\rangle \equiv |n_1, n_2, n_3\rangle$, total $\beta = 4$ in number, can be uniquely identified by the row-state quantum number m . It is evident that the quantum number m does not vary uniformly, and is thus unsuitable as labels of the row states in further computations. So, a uniformly spaced index i is used to tag the row states. As shown in Table II, the index i is ordered as per the sequential ordering in quantum number m such that $i = 1$ represents row state with the lowest value of m , $i = 2$ corresponds to the row state with the second lowest value of m , and so on.

$ \phi_m\rangle \equiv$ $ n_1 \ n_2 \ n_3\rangle$	$ 1 \ 1 \ 1\rangle$	$ 2 \ 1 \ 1\rangle$	$ 1 \ 2 \ 1\rangle$	$ 1 \ 1 \ 2\rangle$
m	13	14	16	22
i	1	2	3	$\beta = 4$

TABLE II. Table showing all possible row-state configurations together with the corresponding values of the row-state quantum number m and state index i .

Next, we consider the two-row states $|\Phi_M^2\rangle$ generated from the direct product of the row states $|\phi_{m_1}\rangle$ and $|\phi_{m_2}\rangle$, chosen from the row-state configurations shown in Table II. At this stage, the possible two-row states can be filtered by constraining the total number of bosons within the two rows to be at-most 10, since this is the maximum number of bosons within the 3×3 lattice. With this constraint, all possible two-row states configurations are $\beta^{(2)} = 16$ in number, and are shown in Table III. Similar to the case of previously constructed row states, the quantum number M does not vary uniformly and is thus not used for enumeration purpose. Instead, we tag each of the two-row states with a uniformly spaced index I , which is sequenced in accordance with the quantum numbers of the two contributing row states (m_1, m_2) , with m_2 as the faster varying index.

Finally, the basis states corresponding to the system of $N = 10$ particles on a 3×3 lattice is constructed from the direct product of the rowstate $|\phi_{m_3}\rangle$ and the two-row state $|\Phi_M^2\rangle$, constructed earlier and shown in Table II and III. Out of all possible combinations, valid basis states are enumerated by filtering out only those states for which the total number of particles in the 3×3 lattice is fixed as $N = 10$. Table IV lists all such possible basis states, which are Γ in number. Again, similar to the previous cases, the basis states are tagged

$ \Phi_M^2\rangle = \begin{matrix} \phi_{m_2}\rangle \\ \otimes \\ \phi_{m_1}\rangle \end{matrix}$	$\mathbf{M} = (m_1, m_2)$	$M = \ \mathbf{M}\ $	I
$\begin{vmatrix} 1 & 1 & 1 \\ 1 & 1 & 1 \end{vmatrix}$	(13, 13)	364	1
$\begin{vmatrix} 2 & 1 & 1 \\ 1 & 1 & 1 \end{vmatrix}$	(13, 14)	365	2
$\begin{vmatrix} 1 & 2 & 1 \\ 1 & 1 & 1 \end{vmatrix}$	(13, 16)	367	3
$\begin{vmatrix} 1 & 1 & 2 \\ 1 & 1 & 1 \end{vmatrix}$	(13, 22)	373	4
$\begin{vmatrix} 1 & 1 & 1 \\ 2 & 1 & 1 \end{vmatrix}$	(14, 13)	391	5
$\begin{vmatrix} 2 & 1 & 1 \\ 2 & 1 & 1 \end{vmatrix}$	(14, 14)	392	6
$\begin{vmatrix} 1 & 2 & 1 \\ 2 & 1 & 1 \end{vmatrix}$	(14, 16)	394	7
$\begin{vmatrix} 1 & 1 & 2 \\ 2 & 1 & 1 \end{vmatrix}$	(14, 22)	400	8
$\begin{vmatrix} 1 & 1 & 1 \\ 1 & 2 & 1 \end{vmatrix}$	(16, 13)	445	9
$\begin{vmatrix} 2 & 1 & 1 \\ 1 & 2 & 1 \end{vmatrix}$	(16, 14)	446	10
$\begin{vmatrix} 1 & 2 & 1 \\ 1 & 2 & 1 \end{vmatrix}$	(16, 16)	448	11
$\begin{vmatrix} 1 & 1 & 2 \\ 1 & 2 & 1 \end{vmatrix}$	(16, 22)	454	12
$\begin{vmatrix} 1 & 1 & 1 \\ 1 & 1 & 2 \end{vmatrix}$	(22, 13)	607	13
$\begin{vmatrix} 2 & 1 & 1 \\ 1 & 1 & 2 \end{vmatrix}$	(22, 14)	608	14
$\begin{vmatrix} 1 & 2 & 1 \\ 1 & 1 & 2 \end{vmatrix}$	(22, 16)	610	15
$\begin{vmatrix} 1 & 1 & 2 \\ 1 & 1 & 2 \end{vmatrix}$	(22, 22)	616	$\beta^{(2)} = 16$

TABLE III. Table showing all possible two-row states configurations with the corresponding vector label \mathbf{M} for the constraint of atmost 10 particles within 2 rows. The quantum number $M = \|\mathbf{M}\|$ is given by Eq. (8).

with uniformly varying index I which is sequenced in accordance with the quantum numbers of contributing row states (m_1, m_2, m_3) , with m_1 being slowest varying while m_3 as fastest varying index.

Appendix B: Additional details regarding the T_{ED} computations

For comparison of T_{ED} shown in Fig. 5 and 6, the codes were executed on a cluster computer with 256GB RAM per node. In the Fig. 5, we compare the execution time of our ED code (written in FORTRAN) against the “quantum ba-

$ \Phi_M^3\rangle = \begin{matrix} \phi_{m_3}\rangle \\ \otimes \\ \phi_{m_2}\rangle \\ \otimes \\ \phi_{m_1}\rangle \end{matrix}$	$\mathbf{M} = (m_1, m_2, m_3)$	$M = \ \mathbf{M}\ $	I
$\begin{vmatrix} 2 & 1 & 1 \\ 1 & 1 & 1 \\ 1 & 1 & 1 \end{vmatrix}$	(13, 13, 14)	9842	1
$\begin{vmatrix} 1 & 2 & 1 \\ 1 & 1 & 1 \\ 1 & 1 & 1 \end{vmatrix}$	(13, 13, 16)	9844	2
$\begin{vmatrix} 1 & 1 & 2 \\ 1 & 1 & 1 \\ 1 & 1 & 1 \end{vmatrix}$	(13, 13, 22)	9850	3
$\begin{vmatrix} 1 & 1 & 1 \\ 2 & 1 & 1 \\ 1 & 1 & 1 \end{vmatrix}$	(13, 14, 13)	9868	4
$\begin{vmatrix} 1 & 1 & 1 \\ 1 & 2 & 1 \\ 1 & 1 & 1 \end{vmatrix}$	(13, 16, 13)	9922	5
$\begin{vmatrix} 1 & 1 & 1 \\ 1 & 1 & 2 \\ 1 & 1 & 1 \end{vmatrix}$	(13, 22, 13)	10084	6
$\begin{vmatrix} 1 & 1 & 1 \\ 1 & 1 & 1 \\ 2 & 1 & 1 \end{vmatrix}$	(14, 13, 13)	10570	7
$\begin{vmatrix} 1 & 1 & 1 \\ 1 & 1 & 1 \\ 1 & 2 & 1 \end{vmatrix}$	(16, 13, 13)	12028	8
$\begin{vmatrix} 1 & 1 & 1 \\ 1 & 1 & 1 \\ 1 & 1 & 2 \end{vmatrix}$	(22, 13, 13)	16402	$\Gamma = 9$

TABLE IV. Table showing all possible basis states identified by the corresponding vector label \mathbf{M} for a system of ten particles on a 3×3 lattice.

sis” code. The later code is written in C language and utilizes the concept of “Lin Tables” for basis identification. And, the matrix diagonalization is possible with either Lanczos method or with implicitly restarted Arnoldi method using ARPACK package. Using the Lanczos diagonalization procedure in “quantum basis”, we note that the ground state is identical to the value obtained from our method. For comparing the two methods, we consider the T_{ED} using the ARPACK method. For the results shown in Fig. 5, the two codes were executed sequentially. And, for T_{ED} comparison shown in Fig. 6, the ED code was executed on two threads.

- [1] P. M. Chaikin and T. C. Lubensky, *Principles of Condensed Matter Physics* (Cambridge University Press, 1995).
- [2] Anders W. Sandvik and Juhani Kurkijärvi, “Quantum monte carlo simulation method for spin systems,” *Phys. Rev. B* **43**, 5950–5961 (1991).
- [3] A W Sandvik, “A generalization of handscomb’s quantum monte carlo scheme-application to the 1d hubbard model,” *Journal of Physics A: Mathematical and General* **25**, 3667 (1992).
- [4] Patrik Henelius and Anders W. Sandvik, “Sign problem in monte carlo simulations of frustrated quantum spin systems,” *Phys. Rev. B* **62**, 1102–1113 (2000).
- [5] Cornelius Lanczos, “Solution of systems of linear equations by minimized iterations,” *J. Res. Nat. Bur. Standards* **49**, 33–53 (1952).
- [6] D. Calvetti, L. Reichel, and D. C. Sorensen, “An implicitly restarted lanczos method for large symmetric eigenvalue problems,” *Electron. Trans. Numer. Anal.* **2**, 1–21 (1994).
- [7] Andreas M. Läuchli, Julien Sudan, and Erik S. Sørensen, “Ground-state energy and spin gap of spin- $\frac{1}{2}$ kagomé-heisenberg antiferromagnetic clusters: Large-scale exact diagonalization results,” *Phys. Rev. B* **83**, 212401 (2011).
- [8] Andreas M. Läuchli, Julien Sudan, and Roderich Moessner, “ $s = \frac{1}{2}$ kagome heisenberg antiferromagnet revisited,” *Phys. Rev. B* **100**, 155142 (2019).
- [9] Rukmani Bai, Soumik Bandyopadhyay, Sukla Pal, K. Suthar, and D. Angom, “Bosonic quantum hall states in single-layer two-dimensional optical lattices,” *Phys. Rev. A* **98**, 023606 (2018).
- [10] Maciej Lewenstein, Anna Sanpera, and Verònica Ahufinger, *Ultracold Atoms in Optical Lattices: Simulating quantum many-body systems* (Oxford University Press, 2012).
- [11] M. Greiner, O. Mandel, T. Esslinger, T. W. Hänsch, and I. Bloch, “Quantum phase transition from a superfluid to a Mott insulator in a gas of ultracold atoms,” *Nature (London)* **415**, 39 (2002).
- [12] M. Lewenstein, A. Sanpera, V. Ahufinger, B. Damski, A. Sen(De), and U. Sen, “Ultracold atomic gases in optical lattices: mimicking condensed matter physics and beyond,” *Adv. Phys.* **56**, 243 (2007).
- [13] J. Hubbard, “Electron correlations in narrow energy bands,” *Proc. Royal Soc. A* **276**, 238 (1963).
- [14] M. P. A. Fisher, P. B. Weichman, G. Grinstein, and D. S. Fisher, “Boson localization and the superfluid-insulator transition,” *Phys. Rev. B* **40**, 546 (1989).
- [15] D. Jaksch, C. Bruder, J. I. Cirac, C. W. Gardiner, and P. Zoller, “Cold bosonic atoms in optical lattices,” *Phys. Rev. Lett.* **81**, 3108 (1998).
- [16] D. S. Rokhsar and B. G. Kotliar, “Gutzwiller projection for bosons,” *Phys. Rev. B* **44**, 10328 (1991).
- [17] K. Sheshadri, H. R. Krishnamurthy, R. Pandit, and T. V. Ramakrishnan, “Superfluid and insulating phases in an interacting-boson model: Mean-field theory and the RPA,” *EPL* **22**, 257 (1993).
- [18] M. Ö. Oktel, M. Niğ ä, and B. Tanatar, “Mean-field theory for Bose-Hubbard model under a magnetic field,” *Phys. Rev. B* **75**, 045133 (2007).
- [19] M. Aidelsburger, M. Atala, S. Nascimbène, S. Trotzky, Y.-A. Chen, and I. Bloch, “Experimental realization of strong effective magnetic fields in an optical lattice,” *Phys. Rev. Lett.* **107**, 255301 (2011).
- [20] M. Aidelsburger, M. Atala, M. Lohse, J. T. Barreiro, B. Paredes, and I. Bloch, “Realization of the Hofstadter Hamiltonian with ultracold atoms in optical lattices,” *Phys. Rev. Lett.* **111**, 185301 (2013).
- [21] K. Jiménez-García, L. J. LeBlanc, R. A. Williams, M. C. Beeler, A. R. Perry, and I. B. Spielman, “Peierls substitution in an engineered lattice potential,” *Phys. Rev. Lett.* **108**, 225303 (2012).
- [22] Jean Dalibard, Fabrice Gerbier, Gediminas Juzeliūnas, and Patrik Öhberg, “Colloquium: Artificial gauge potentials for neutral atoms,” *Rev. Mod. Phys.* **83**, 1523–1543 (2011).
- [23] M Aidelsburger, “Artificial gauge fields and topology with ultracold atoms in optical lattices,” *Journal of Physics B: Atomic, Molecular and Optical Physics* **51**, 193001 (2018).
- [24] N. R. Cooper, J. Dalibard, and I. B. Spielman, “Topological bands for ultracold atoms,” *Rev. Mod. Phys.* **91**, 015005 (2019).
- [25] Philipp Hauke and Iacopo Carusotto, “Quantum hall and synthetic magnetic-field effects in ultra-cold atomic systems,” in *Encyclopedia of Condensed Matter Physics (Second Edition)*, edited by Tapash Chakraborty (Academic Press, Oxford, 2024) second edition ed., pp. 629–639.
- [26] Julian Léonard, Sooshin Kim, Joyce Kwan, Perrin Segura, Fabian Grusdt, Cécile Repellin, Nathan Goldman, and Markus Greiner, “Realization of a fractional quantum hall state with ultracold atoms,” *Nature* **619**, 495–499 (2023).
- [27] Rukmani Bai, Soumik Bandyopadhyay, Sukla Pal, K. Suthar, and D. Angom, “Quantum hall states for $\alpha = 1/3$ in optical lattices,” in *Quantum Collisions and Confinement of Atomic and Molecular Species, and Photons* (Springer Singapore, 2019) pp. 211–221.
- [28] Deepak Gaur, Hrushikesh Sable, and D. Angom, “Fractional quantum hall effect in optical lattices,” *Frontiers in Physics* **10** (2023), 10.3389/fphy.2022.1106491.
- [29] S. Pal, R. Bai, S. Bandyopadhyay, K. Suthar, and D. Angom, “Enhancement of the bose glass phase in the presence of an artificial gauge field,” *Phys. Rev. A* **99**, 053610 (2019).
- [30] K. Suthar, Hrushikesh Sable, Rukmani Bai, Soumik Bandyopadhyay, Sukla Pal, and D. Angom, “Supersolid phase of the extended bose-hubbard model with an artificial gauge field,” *Phys. Rev. A* **102**, 013320 (2020).
- [31] Kuldeep Suthar, Rebecca Kraus, Hrushikesh Sable, Dilip Angom, Giovanna Morigi, and Jakub Zakrzewski, “Staggered superfluid phases of dipolar bosons in two-dimensional square lattices,” *Phys. Rev. B* **102**, 214503 (2020).
- [32] Rukmani Bai, Deepak Gaur, Hrushikesh Sable, Soumik Bandyopadhyay, K. Suthar, and D. Angom, “Segregated quantum phases of dipolar bosonic mixtures in two-dimensional optical lattices,” *Phys. Rev. A* **102**, 043309 (2020).
- [33] Soumik Bandyopadhyay, Hrushikesh Sable, Deepak Gaur, Rukmani Bai, Subroto Mukerjee, and D. Angom, “Quantum phases of dipolar bosons in a multilayer optical lattice,” *Phys. Rev. A* **106**, 043301 (2022).
- [34] Alexei Kitaev and John Preskill, “Topological entanglement entropy,” *Phys. Rev. Lett.* **96**, 110404 (2006).
- [35] Michael Levin and Xiao-Gang Wen, “Detecting topological order in a ground state wave function,” *Phys. Rev. Lett.* **96**, 110405 (2006).
- [36] Konstantin V. Krutitsky, “Ultracold bosons with short-range interaction in regular optical lattices,” *Physics Reports* **607**, 1–101 (2016), ultracold bosons with short-range interaction in regular optical lattices.

- [37] D.-S. Lühmann, “Cluster Gutzwiller method for bosonic lattice systems,” *Phys. Rev. A* **87**, 043619 (2013).
- [38] Rukmani Bai, *Synthetic Magnetic Fields and Multi-Component BECs in Optical Lattices*, Ph.D. thesis, Indian Institute of Technology Gandhinagar (2018).
- [39] Barbara Capogrosso-Sansone, Şebnem Güneş Söyler, Nikolay Prokof’ev, and Boris Svistunov, “Monte carlo study of the two-dimensional bose-hubbard model,” *Phys. Rev. A* **77** (2008), 10.1103/PhysRevA.77.015602.
- [40] The QMC data is obtained from personal communication with Prof. Barbara Capogrosso-Sansone.
- [41] Zhentao Wang, “Quantum basis: Exact diagonalization library for general models, https://github.com/wztzjhn/quantum_basis,” .
- [42] Artur Ekert and Peter L. Knight, “Entangled quantum systems and the Schmidt decomposition,” *American Journal of Physics* **63**, 415–423 (1995), https://pubs.aip.org/aapt/ajp/article-pdf/63/5/415/11806926/415_1_online.pdf.
- [43] J. Eisert, M. Cramer, and M. B. Plenio, “Colloquium: Area laws for the entanglement entropy,” *Rev. Mod. Phys.* **82**, 277–306 (2010).
- [44] Jiang-Min Zhang and Yu Liu, “Geometric entanglement in the Laughlin wave function,” *New Journal of Physics* **19**, 083019 (2017).
- [45] D. Jaksch and P. Zoller, “Creation of effective magnetic fields in optical lattices: the Hofstadter butterfly for cold neutral atoms,” *New J. Phys.* **5**, 56 (2003).
- [46] X. G. Wen and Q. Niu, “Ground-state degeneracy of the fractional quantum hall states in the presence of a random potential and on high-genus Riemann surfaces,” *Phys. Rev. B* **41**, 9377–9396 (1990).
- [47] Yasuhiro Hatsugai, “Characterization of topological insulators: Chern numbers for ground state multiplet,” *Journal of the Physical Society of Japan* **74**, 1374–1377 (2005), <https://doi.org/10.1143/JPSJ.74.1374>.
- [48] K. J. Maschhoff and D. C. Sorensen, “P_arpack: An efficient portable large scale eigenvalue package for distributed memory parallel architectures,” in *Applied Parallel Computing Industrial Computation and Optimization*, edited by Jerzy Waśniewski, Jack Dongarra, Kaj Madsen, and Dorte Olsen (Springer Berlin Heidelberg, Berlin, Heidelberg, 1996) pp. 478–486.